electronics

Article

Study of an Attenuator Supporting Meander-Line Slow Wave Structure for Ka-Band TWT

Hexin Wang [1], Shaomeng Wang [1,*], Zhanliang Wang [1], Xinyi Li [2], Tenglong He [1], Duo Xu [1], Zhaoyun Duan [1], Zhigang Lu [1], Huarong Gong [1] and Yubin Gong [1,*]

[1] National Key Lab on Vacuum Electronics, University of Electronic Science and Technology of China, Chengdu 610054, China; whx427@126.com (H.W.); wangzl@uestc.edu.cn (Z.W.); faithhill@foxmail.com (T.H.); xuduo1234567@hotmail.com (D.X.); zhyduan@uestc.edu.cn (Z.D.); lzhgchnn@uestc.edu.cn (Z.L.); hrgong@uestc.edu.cn (H.G.)

[2] Nanjing Sanle Electronic Group Co., Ltd., Nanjing 211800, China; leexy222@163.com

* Correspondence: wangsm@uestc.edu.cn (S.W.); ybgong@uestc.edu.cn (Y.G.); Tel.: +86-137-0900-5056 (S.W.); +86-138-0803-6055 (Y.G.)

Abstract: An attenuator supporting meander-line (ASML) slow wave structure (SWS) is proposed for a Ka-band traveling wave tube (TWT) and studied by simulations and experiments. The ASML SWS simplifies the fabrication and assembly process of traditional planar metal meander-lines (MLs) structures, by employing an attenuator to support the ML on the bottom of the enclosure rather than welding them together on the sides. To reduce the surface roughness of the molybdenum ML caused by laser cutting, the ML is coated by a thin copper film by magnetron sputtering. The measured S_{11} of the ML is below −20 dB and S_{21} varies around −8 dB to −12 dB without the attenuator, while below −40 dB with the attenuator. Particle-in-cell (PIC) simulation results show that with a 4.4-kV, 200-mA sheet electron beam, a maximum output power of 126 W is obtained at 38 GHz, corresponding to a gain of 24.1 dB and an electronic efficiency of 14.3%, respectively.

Keywords: meander-line; surface roughness; S-parameters; slow wave structure; traveling wave tube

Citation: Wang, H.; Wang, S.; Wang, Z.; Li, X.; He, T.; Xu, D.; Duan, Z.; Lu, Z.; Gong, H.; Gong, Y. Study of an Attenuator Supporting Meander-Line Slow Wave Structure for Ka-Band TWT. *Electronics* **2021**, *10*, 2372. https://doi.org/10.3390/electronics10192372

Academic Editor: Yahya M. Meziani

Received: 16 August 2021
Accepted: 26 September 2021
Published: 28 September 2021

1. Introduction

With the large-scale application of 5G communication networks and the rapid development of 6G, the demands for high-power, high-efficiency millimeter wave sources are increasing rapidly [1–5] in recent years. Compared with the widely used solid-state power amplifiers (SSPAs), the traveling wave tube has inherent advantages at a millimeter wave frequency, such as generating high-power electromagnetic waves easily and with high efficiency and an excellent heat dissipation ability [6–9].

However, the traditional TWT usually has disadvantages, such as large size and weight, high operation voltage and so on, which make it difficult to meet the requirements of the communication industry for miniaturization and mass production. As a result, the planar slow wave structure (SWS) has attracted wide attention over the last decade. One kind of self-winding helix quasi-planar SWS is explored and fabricated by using MEMS technology for potential mass production [10]. The planar SWS features as almost two-dimensional rather than three-dimensional. The typical planar SWS, formed by periodically bending a thin metal line on the dielectric substrate, is a kind of microstrip meander line. This process can be seen as flattening the traditional helix SWS into a flat structure. In the category of planar SWSs, many different bending forms, such as V-shaped [11], U-shaped [12], angular log-periodic [13], coplanar [14], etc., have been proposed successively.

The microstrip SWSs have the advantages of a low operation voltage and easy fabrication by using semiconductor technology for mass production, yet there are some problems needing to be solved before applying them in practice to TWTs. For example, the metal layer is usually too thin (less than 10 μm) to withstand the heat generated by high energy electrons bombardments [15], and the accumulating charges on the dielectric substrate tend to damage the SWSs [16].

Therefore, a meander-line (ML) SWS supported by side dielectric rods instead of a bottom substrate slab was proposed [17] and furtherly developed with different patterns [18,19]. The ML which was cut off from a metal sheet by laser is much thicker (~200 μm) than those fabricated by magnetron sputtering. As a result, it not only inherits the advantages of the low voltage and small size of the microstrip type SWSs, but also solves the problems mentioned above. Based on this, the staggered dual ML SWS supported by side dielectric rods is proposed in [20], in which the simulation results show it can generate 283 W at 75 GHz. In addition, the diamond bottom supported ML SWSs are also studied and fabricated in the Ka-band [21] and X-band [22], in which the measurement of transmission characteristics shows a comparable agreement with the simulations. In [23], a new fabrication method to make the side dielectric rods supporting the ML SWS, is explored by using mechanical roll bending of the copper strip. However, there was a problem found on the ML SWS, that the feasibility was difficult to guarantee when welding the metal meander line and dielectric rods. The assembly process is still complex.

Therefore, in order to simplify the assembly process, a novel attenuator supporting meander-line (ASML) SWS is presented in this paper. Its main feature is using the dielectric attenuator block to support the ML at the bottom, instead of welding them together on the side, which makes the connection between the ML and dielectric rods much easier. Instead of using traditional helix rods with an attenuator, the dielectric attenuator block simplifies the assembly process and retains the function to absorb the backward oscillation at the same time. In addition, by reducing the distance between the bottom metal shield and the ML, the operation voltage is further reduced. According to the simulation results, with the electron beam voltage of 4.4 kV, an output power of 126 W can be obtained from the ASML SWS TWT, with a maximum gain and electronic efficiency of 24.1 dB and 14.3%, respectively.

In addition, the fabrication processing and the measurement of the surface roughness and reflection-transmission characteristics of this structure are discussed. By using a laser confocal microscope to measure the surface roughness, it is verified that the surface roughness has been improved after copper coating on the ML's original material of molybdenum (Mo). The measured S-parameters characteristics of the SWS shows during the designed band of 36–39 GHz, the S_{11} is below -20 dB and the S_{21} of the ML varies around -8 to -12 dB and the S_{21} of the attenuator is below -40 dB. This new structure inherits the characteristics of the ML, such as high output power, planarization and low working voltage, further reducing the difficulty of processing and assembly which makes it easier to manufacture and mass produce.

The rest of the paper is organized as follows: in Section 2, the structure model and parameters are presented, as well as the high frequency characteristics of the ASML SWS. In Section 3, the input and output structures are designed and fabrication issues are discussed. In addition, the surface roughness and S-parameters measurement results are presented and analyzed. In Section 4, the results of beam-wave interaction obtained from particle-in-cell (PIC) simulation are shown to predict the potential performance of a TWT based on the ASML SWS. At the end, Section 5 gives the conclusion of the article.

2. Structure Model and High Frequency Characteristics of the ASML SWS

In order to study the dispersion characteristics of the ASML, a single period model is established. Figure 1 shows the perspective view of the one-period structure with labelled dimensional parameters and the cross-sectional view showing the relative positions of the meander-line, electron beam and metal shield, respectively. The metal meander-line is in a U shape with right angle corners. The thickness of the meander-lines is t, the width is a, and the length of the long arms is d. The distance between the adjacent straight lines is j, so the length of a single period in z direction is $p = 2 \times (a + j)$.

The height of the metal shield is *ay*, the distance from the bottom metal shield is *dy*. When *dy* is small, it can be regarded as loading the ridge on the bottom layer, which reduces the working voltage.

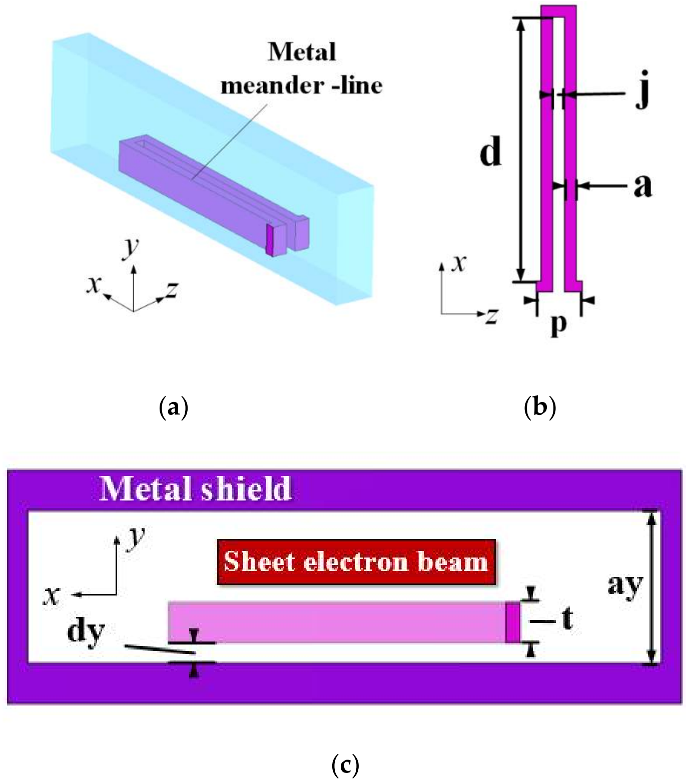

Figure 1. The different view of one period of the ASML SWS in the (**a**) 3-D, (**b**) xz plane and (**c**) xy plane.

Different from the PDU-MML SWS [12], this kind of SWS is supported from the bottom by the attenuator located around the middle of the SWS instead of welding the line and dielectric rods, as shown in Figure 2. Similar to the fabrication of the conventional helix TWTs, the attenuator can be obtained by evaporating a carbon film on the boron nitride (BN) block easily. The dimensional parameters' values after optimization are provided in Table 1.

Table 1. The critical dimensional parameters of the ASML SWS.

Parameters	Value (mm)	Parameters	Value (mm)
d	1.6	*ay*	0.756
a	0.07	*dy*	0.1
j	0.07	*d1*	0.7
p	0.28	*d2*	0.2
t	0.2	*d3*	0.4

The dispersion curves of the ASML SWS are calculated by using the eigenmode solver of the commercial simulation software CST STUDIO SUITE. For the dimension values in Table 1, the effects of *dy* on the dispersion curves are investigated and plotted in Figure 3a. It can be seen that the curves become flat when *dy* reduces, which means the phase velocity of the electromagnetic wave is becoming smaller. Finally, the *dy* = 0.1 mm is used in the later TWT design. The Figure 3b indicates the interaction impedance is above 40 Ohms from 10–40 GHz.

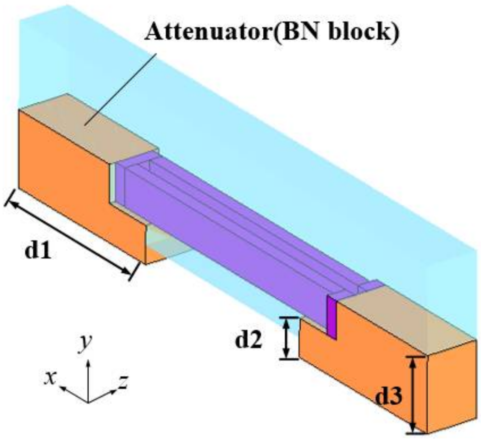

Figure 2. Geometry of the attenuator part in 3-D view.

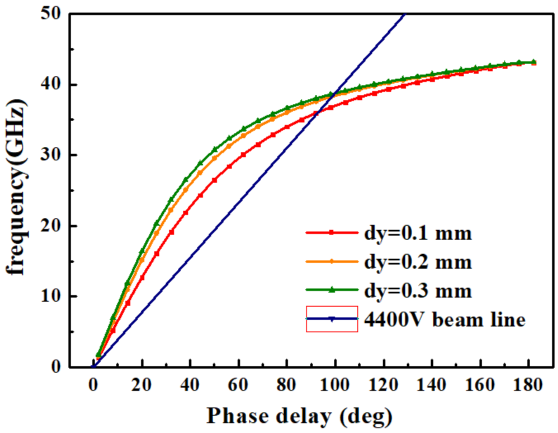

(**a**)

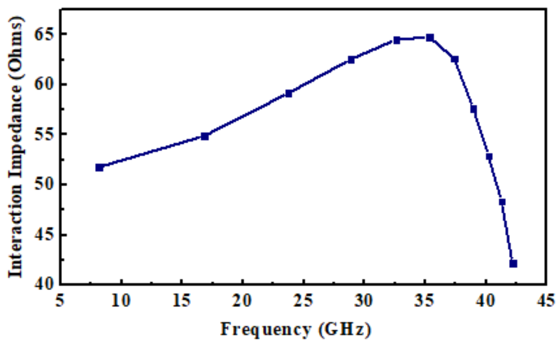

(**b**)

Figure 3. (**a**) The dispersion curves versus frequency for different values of dy and (**b**) the interaction impedance.

3. Fabrication and Measurement Issues

3.1. Fabrication and Assembly

Figure 4a gives the assembly sketch of the ASML SWS, and as can be seen, the metal enclosures (pink parts) with transition stepped ridge waveguides and flanges are fabricated together with the same processing in order to reduce the assembly error as much as possible. The upper and lower metal enclosures will be fixed by the clamps (blue parts). As for the metal meander-line, the fabrication process contains two steps. The first step is through the picosecond laser cutting molybdenum sheet to fabricate the required pattern of the ML.

The second step is covering the whole ML with a thin copper film (~3 μm) by magnetron sputtering, which can improve the surface roughness and the conductivity of the ML.

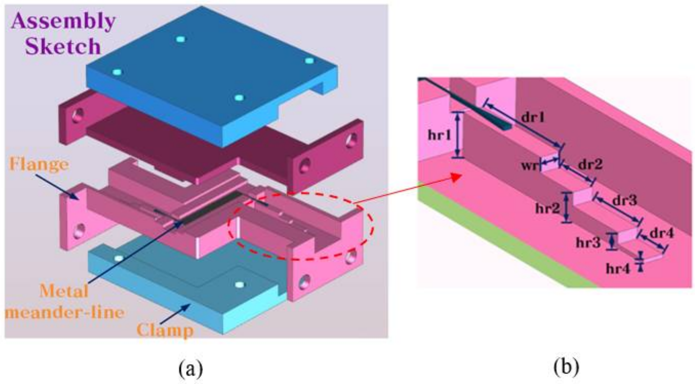

Figure 4. (**a**) The assembly sketch of ASML SWS with clamp, (**b**) the input-output couplers of the stepped ridge waveguide transition.

In order to connect the ASML SWS to a standard WR-28 rectangular waveguide (3.556 mm × 7.112 mm), the stepped ridge waveguide to strip line transition that could gradually transform the TE_{10} waveguide mode to quasi-TEM mode has been proposed as input-output couplers for beam-wave interaction. Figure 4b shows the half part of the SWS and the detailed transition structure with main dimensional parameters for designing the suitable mode converter. The values of the transition structure are listed in Table 2.

Table 2. The main dimensions of the staggered stepped ridge waveguide transition.

Parameters	Values (mm)	Parameters	Values (mm)
dr1	6	*hr1*	2.3
dr2	2.55	*hr2*	1.5
dr3	3.5	*hr3*	0.8
dr4	2	*hr4*	0.2
wr	1.1	-	-

Figure 5 shows the fabricated SWS, in which the ML has already connected with the ridge of the input-output couplers by using spot welding. There are two sets of SWSs fabricated for measuring the main transmission loss of the ML with and without the attenuator, respectively. One is the ML with normal BN block (white block in Figure 5a). The other is the ML with the attenuator block that is fabricated by evaporating carbon on a BN block, which is shown in Figure 5b.

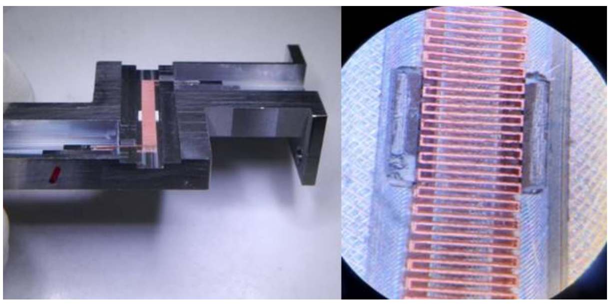

(**a**) (**b**)

Figure 5. The two sets of the fabricated SWSs, (**a**) the ML with normal BN block, (**b**) ML with attenuator block.

3.2. The Surface Roughness Measurement

To demonstrate the improvement on the surface roughness after magnetron sputtering of the copper film on the Mo meander-line, the values of roughness are measured by using a laser confocal microscope (Olympus LEXT 5000). Because the ML is cut by the laser from the top, the side surfaces are much rougher than the top surface. Figure 6a shows the side surface of the Mo ML, in which the laser cutting strip marks are obvious. The surface roughness of three random sample points varies from 410 to 670 nm. Figure 6b shows the side surface of the Mo ML after the copper film sputtering. It can be seen that the laser cutting marks are not obvious, and the values vary from 220 to 360 nm. As for the top surface of the ML, the surface roughness of the Mo ML varies from 90 to 170 nm, and the Mo ML with copper film varies from 70 to 120 nm.

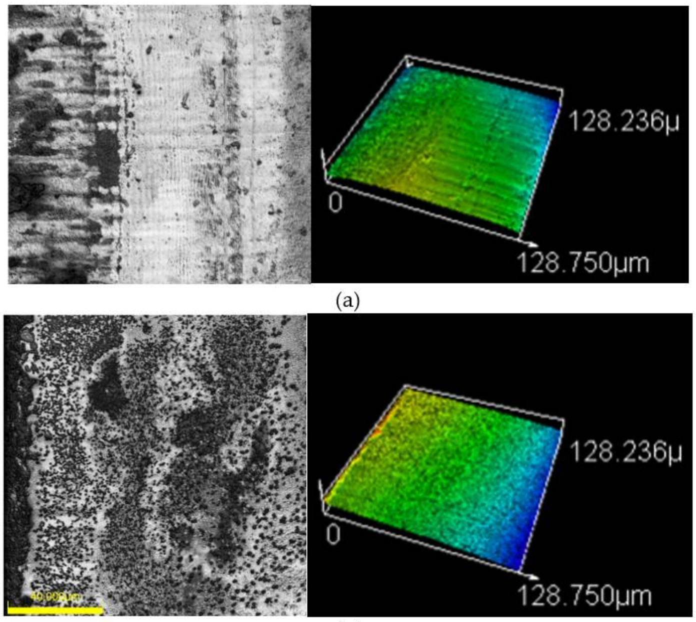

(b)

Figure 6. Test image of surface roughness by Olympus LEXT 5000 at the side surface of (**a**) Mo ML and (**b**) Mo ML with copper film.

According to the calculation equation of effective conductivity (σ_{ef}), Equation (1) [24],

$$\sigma_{ef} = \frac{\sigma}{(1 + \frac{2}{\pi}\arctan(1.4 \times (\frac{R_S}{\delta})^2))^2} \tag{1}$$

It can be seen that the effective conductivity can be improved by two aspects. One is increasing the material conductivity, as the conductivity of copper (5.8×10^7 S/m) is much better than that of Mo (2×10^7 S/m); the other one is to reduce the surface roughness (R_S) that is improved by coating copper as demonstrated above. The δ is skin depth, which is 339 nm at 38 GHz. According to the measured surface roughness, the effective conductivity of the ML with copper film is calculated to be around 3×10^7 S/m.

3.3. S-Parameters Measurements

To study the reflection-transmission characteristics of the 54-period ML with BN block and attenuator block supporting, respectively, two sets of SWSs are fabricated (Figure 5) and measured (Figure 7). For comparison, the simulations are also conducted by using CST STUDIO SUITE, in which the conductivity of the ML varies from 2×10^7 S/m to 5×10^7 S/m. The relative permittivity and loss tangent of the BN material are set as ε_r = 4 and tanδ = 0.0005, respectively.

The comparisons of the measured and simulated S_{11} and S_{21} results are shown in Figure 8a. The S_{11} results show a good agreement between the measured and simulated results, which is below −20 dB from the designed frequency band of 36 GHz to 40 GHz. As for the S_{21}, the measured result varies around −8 dB to −12 dB from 36 GHz to 39 GHz, which shows a good agreement with the simulation of conductivity of 3×10^7 S/m. In addition, this result also approximately meets the result calculated by using the surface roughness measurement results.

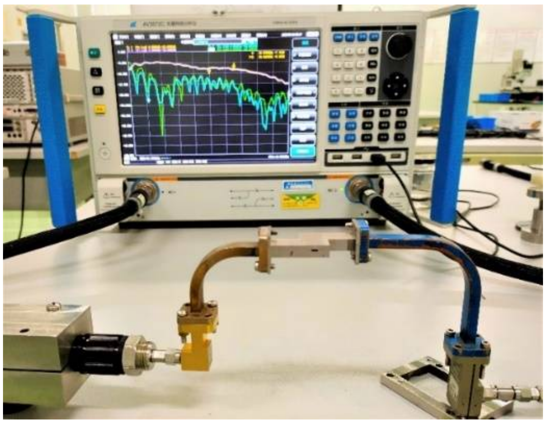

Figure 7. The measurement of S-parameters by using a vector network analyzer.

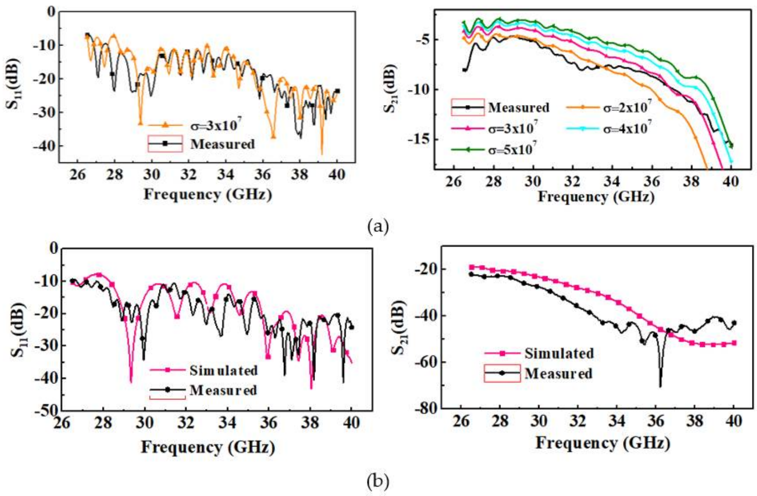

Figure 8. The comparison of S-parameters of the ML SWS with (**a**) BN block supporting and (**b**) attenuator supporting.

As for the ML with attenuator support, the relative permittivity of the attenuator is set to ε_r = 4 and the loss tangent is set to tanδ = 0.5 in the simulation. According to Figure 8b, it can be seen that the S_{11} stays approximately the same between the measured and the simulated results, with or without the attenuator. With regard to the S_{21}, during the 35–39 GHz, the measured and the simulated results are both below −40 dB, which means that the attenuator absorbs the majority of the wave energy and works well.

4. "Hot" Performance of the ASML TWT

To fully study the beam-wave interaction characteristics of the ASML TWT, 3-D particle-in-cell (PIC) simulations are carried out by CST PARTICLE STUDIO. A sheet electron beam with an operation voltage and current of 4.4 kV and 200 mA is used in the simulation. The cross-sectional dimensions of the sheet-beam are 960 µm × 100 µm with a current density of 208 A/cm^2. A solenoid magnetic field of 0.4 T is used to maintain the transmission of the sheet electron beam. The conductivity of the metal line is set to $\sigma = 3 \times 10^7$ S/m for eventual ohmic losses due to surface roughness.

Figure 9 shows the time and frequency domain information of the output signal at 38 GHz, in which an input signal with an average power of 0.5 W is used. After 2 ns the output signal becomes stable with a power of 126 W, corresponding to a maximum gain of 24.1 dB and an electronic efficiency of 14.3%. In the 20 ns simulation time, as shown in Figure 9a, the output signal also stays stable, showing that no oscillation occurred.

The output spectrum in Figure 9b shows the fundamental is 60 dB higher than the second harmonic. The beam trajectories and phase-space diagram of the strongly modulated electron beam are shown in Figure 10. It indicates a strong beam-wave interaction, and the wave gets plenty of energy from the electron beam.

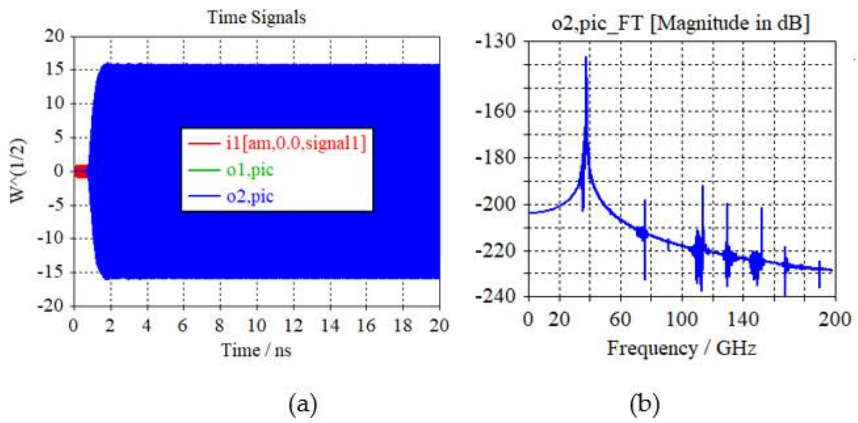

Figure 9. Output signal in (**a**) time-domain and (**b**) frequency-domain.

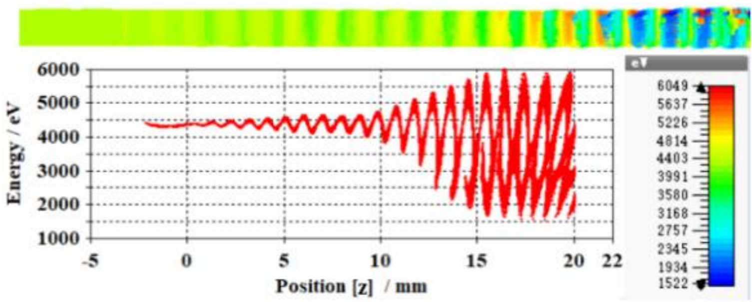

Figure 10. Electron beam bunching and phase space diagram.

Figure 11a shows the output power at 38 GHz as a function of input power with different values of beam current. When the current is 200 A, the output power increased from 5 W to 126 W, as the input power increased from 0.01 W to 0.5 W. However, in the case of the current of 0.1 A, no saturation is observed. In order to study this phenomenon, the further simulation is conducted and the results are shown in Figure 11b, which indicates that the output power at 38 GHz increased from 5 W to 185 W, as the current increased from 0.05 A to 0.25 A, when the input power is 0.5 W. Considering the beam focusing issues, a 0.2 A beam current is used for further study.

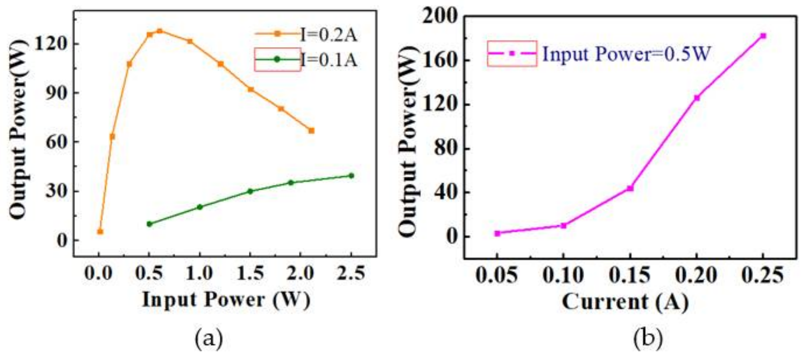

Figure 11. Variation of output power at 38 GHz with (**a**) input power and (**b**) beam current.

Figure 12 shows the variation of the output power with frequency for different beam voltages. The 3-dB hot-bandwidth for 4.4 kV is ~2.5 GHz. Moreover, thanks to the relatively wide cold bandwidth of the ASML, the center frequency can shift from 35 GHz to 40 GHz by changing the beam voltage.

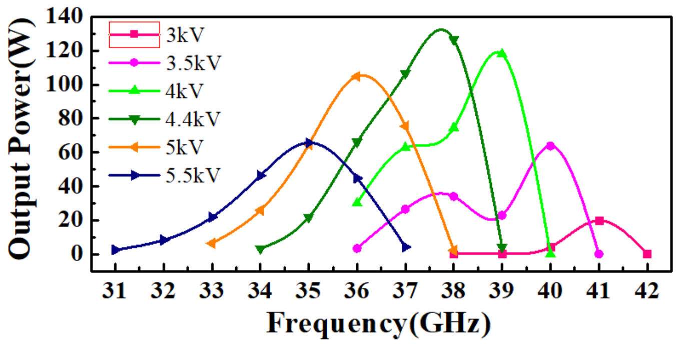

Figure 12. Output power vs. frequency for different beam voltages.

5. Conclusions

The ASML SWS for Ka-band planar TWTs has been proposed and investigated. The structure model and high frequency characteristics of the ASML SWS have been presented. The stepped ridge waveguide to strip-line couplers, which has been designed for connecting the standard Ka-band waveguide, is described. The fabrication of the ML and assembly of the ASML SWS are discussed. To improve the surface roughness of the ML, a thin copper film is coated on the original material Mo by using magnetron sputtering. The surface roughness measurement also verifies this improvement quantitatively. The S-parameters characteristics of the ASML SWS are also studied experimentally. The measured results show that during the designed band of 36–39 GHz, the S_{11} is below -20 dB and the S_{21} of the ML varies around -8 dB to -12 dB and the S_{21} of the SWS with the attenuator is below -40 dB. Furthermore, the "hot" characteristics of the ASML SWS TWT are studied by simulation. The PIC simulation results show the maximum output power of 126 W at 38 GHz is obtained with using a 4.4 kV and 0.2A beam. The maximum gain and electronic efficiency are 24.1 dB and 14.3%, respectively.

Author Contributions: Conceptualization, H.W.; validation, S.W., Z.W.; data curation, X.L., T.H., D.X.; writing—original draft preparation, H.W.; writing—review and editing, Z.D., Z.L., H.G. and Y.G.; supervision, Y.G.; project administration, Y.G. All authors have read and agreed to the published version of the manuscript.

Funding: This work was supported by National Natural Science Foundation of China (NSFC) (Grant Nos. 61921002, 61988102); Science and Technology on High Power Microwave Laboratory Fund (Grant No 6142605180201).

Conflicts of Interest: The authors declare no conflict of interest.

References

1. Jiang, W.; Han, B.; Habibi, M.A.; Schotten, H.D. The Road Towards 6G: A Comprehensive Survey. *IEEE Open J. Commun. Soc.* **2021**, *2*, 334–366. [CrossRef]
2. Hong, W.; Jiang, Z.H.; Yu, C.; Hou, D.; Wang, H.; Guo, C.; Hu, Y.; Kuai, L.; Yu, Y.; Jiang, Z.; et al. The Role of Millimeter-Wave Technologies in 5G/6G Wireless Communications. *IEEE J. Microw.* **2021**, *1*, 101–122. [CrossRef]
3. Liu, Y.; Yuan, X.; Xiong, Z.; Kang, J.; Wang, X.; Niyato, D. Federated learning for 6G communications: Challenges, methods, and future directions. *China Commun.* **2020**, *17*, 9. [CrossRef]
4. Chowdhury, M.Z.; Shahjalal, M.; Ahmed, S.; Jang, Y.M. 6G Wireless Communication Systems: Applications, Requirements, Technologies, Challenges, and Research Directions. *IEEE Open J. Commun. Soc.* **2020**, *1*, 957–975. [CrossRef]
5. Dhillon, S.S.; Vitiello, M.S.; Linfield, E.H.; Davies, A.; Hoffmann, M.; Booske, J.; Paoloni, C.; Gensch, M.; Weightman, P.; Williams, G.P.; et al. The 2017 terahertz science and technology roadmap. *J. Phys. D Appl. Phys.* **2017**, *50*, 043001. [CrossRef]
6. Basu, R.; Rao, J.M.; Le, T.; Letizia, R.; Paoloni, C. Development of a D-Band Traveling Wave Tube for High Data-Rate Wireless Links. *IEEE Trans. Electron Devices* **2021**, *68*, 9. [CrossRef]
7. André, F.; Racamier, J.C.; Zimmermann, R.; Le, Q.T.; Krozer, V.; Ulisse, G.; Minenna, D.F.G.; Letizia, R.; Paoloni, C. Technology, Assembly, and Test of a W -Band Traveling Wave Tube for New 5G High-Capacity Networks. *IEEE Trans. Electron Devices* **2020**, *67*, 7. [CrossRef]
8. Ulisse, G.; Krozer, V. W -Band Traveling Wave Tube Amplifier Based on Planar Slow Wave Structure. *IEEE Electron Device Lett.* **2016**, *38*, 126–129. [CrossRef]
9. Paoloni, C.; Gamzina, D.; Letizia, R.; Zheng, Y.; Luhmann, N.C., Jr. Millimeter wave traveling wave tubes for the 21st Century. *J. Electromagn. Waves Appl.* **2020**, *35*, 567–603. [CrossRef]
10. Prakash, D.J.; Dwyer, M.M.; Argudo, M.M.; Debasu, M.L.; Dibaji, H.; Lagally, M.G.; Van Der Weide, D.W.; Cavallo, F. Self-Winding Helices as Slow-Wave Structures for Sub-Millimeter Traveling-Wave Tubes. *ACS Nano* **2020**, *15*, 1229–1239. [CrossRef] [PubMed]
11. Shen, F.; Wei, Y.; Yin, H.; Gong, Y.; Xu, X.; Wang, S.; Wang, W.; Feng, J. A Novel V-Shaped Microstrip Meander-Line Slow-Wave Structure for W-band MMPM. *IEEE Trans. Plasma Sci.* **2011**, *40*, 463–469. [CrossRef]
12. Shen, F.; Wei, Y.; Xu, X.; Liu, Y.; Huang, M.; Tang, T.; Gong, Y. U-shaped microstrip meander-line slow-wave structure for Ka-band traveling-wave tube. In Proceedings of the 2012 International Conference on Microwave and Millimeter Wave Technology (ICMMT), Shenzhen, China, 5–8 May 2012. [CrossRef]
13. Wang, S.; Gong, Y.; Hou, Y.; Wang, Z.; Wei, Y.; Duan, Z.; Cai, J. Study of a Log-Periodic Slow Wave Structure for Ka-band Radial Sheet Beam Traveling Wave Tube. *IEEE Trans. Plasma Sci.* **2013**, *41*, 2277–2282. [CrossRef]
14. Zhao, C.; Aditya, S.; Wang, S. A Novel Coplanar Slow-Wave Structure for Millimeter-Wave BWO Applications. *IEEE Trans. Electron Devices* **2021**, *68*, 1924–1929. [CrossRef]
15. Ryskin, N.M.; Torgashov, R.A.; Starodubov, A.V.; Rozhnev, A.G.; Serdobintsev, A.A.; Pavlov, A.M.; Galushka, V.V.; Bessonov, D.A.; Ulisse, G.; Krozer, V. Development of microfabricated planar slow-wave structures on dielectric substrates for miniaturized millimeter-band traveling-wave tubes. *J. Vac. Sci. Technol. B* **2021**, *39*, 013204. [CrossRef]
16. Zhao, C.; Aditya, S.; Chua, C. A Microfabricated Planar Helix Slow-Wave Structure to Avoid Dielectric Charging in TWTs. *IEEE Trans. Electron Devices* **2015**, *62*, 1342–1348. [CrossRef]
17. Wang, H.; Wang, Z.; Li, X.; He, T.; Xu, D.; Gong, H.; Tang, T.; Duan, Z.; Wei, Y.; Gong, Y. Study of a miniaturized dual-beam TWT with planar dielectric-rods-support uniform metallic meander line. *Phys. Plasmas* **2018**, *25*, 06. [CrossRef]
18. Dong, Y.; Chen, Z.; Li, X.; Wang, H.; Wang, Z.; Wang, S.; Lu, Z.; Gong, H.; Duan, Z.; Feng, J.; et al. Ka-band dual sheet beam traveling wave tube using supported planar ring-bar slow wave structure. *J. Electromagn. Waves Appl.* **2020**, *34*, 1–15. [CrossRef]
19. Wen, Z.; Luo, J.; Li, Y.; Guo, W.; Zhu, M. A Concentric Arc Meander Line Slow Wave Structure Applied on Low Voltage and High Efficiency Ka-Band TWT. *IEEE Trans. Electron Devices* **2021**, *68*, 1262–1266. [CrossRef]
20. Wang, H.; Wang, S.; Wang, Z.; Li, X.; Xu, D.; Duan, Z.; Lu, Z.; Gong, H.; Aditya, S.; Gong, Y. Dielectric-Supported Staggered Dual Meander-Line Slow Wave Structure for an E-Band TWT. *IEEE Trans. Electron Devices* **2020**, *68*, 369–375. [CrossRef]
21. Wang, Z.; Su, L.; Duan, Z.; Hu, Q.; Gong, H.; Lu, Z.; Feng, J.; Li, S.; Gong, Y. Investigation on a Ka Band Diamond-Supported Meander-Line SWS. *J. Infrared Millim. Terahertz Waves* **2020**, *41*, 1460–1468. [CrossRef]
22. Wang, Z.; Du, F.; Li, S.; Hu, Q.; Duan, Z.; Gong, H.; Gong, Y.; Feng, J. Study on an X-Band Sheet Beam Meander-Line SWS. *IEEE Trans. Plasma Sci. Devices* **2020**, *48*, 12. [CrossRef]
23. Starodubov, A.; Atkin, V.; Torgashov, R.; Navrotsky, I.A.; Ryskin, N. On the technological approach to microfabrication of a meander-line slow-wave structure for millimeter-band traveling-wave tubes with multiple sheet electron beams. In Proceedings of the Saratov Fall Meeting 2020: Laser Physics, Photonic Technologies, and Molecular Modeling, Saratov, Russia, 29 September–2 October 2020.
24. Kirley, M.P.; Booske, J.H. Terahertz conductivity of coppersurfaces. *IEEE Trans. THz Sci. Technol.* **2015**, *6*, 1012–1020. [CrossRef]